doi:10.1016/j.jmb.2005.06.023 J. Mol. Biol. (2005) 351, 417–430

JMB

Available online at www.sciencedirect.com

SCIENCE DIRECT®

ELSEVIER

Conformations of the Signal Recognition Particle Protein Ffh from *Escherichia coli* as Determined by FRET

Iwona Buskiewicz[1], Frank Peske[1], Hans-Joachim Wieden[2] Ignacy Gryczynski[3], Marina V. Rodnina[2] and Wolfgang Wintermeyer[1]*

[1]*Institute of Molecular Biology University of Witten/Herdecke 58448 Witten, Germany*

[2]*Institute of Physical Biochemistry, University of Witten/Herdecke, 58448 Witten Germany*

[3]*Center for Fluorescence Spectroscopy, Department of Biochemistry and Molecular Biology, University of Maryland at Baltimore Baltimore, MD 21201, USA*

**Corresponding author*

The signal recognition particle (SRP) initiates the co-translational targeting of proteins to the plasma membrane in bacteria by binding to the N-terminal signal sequence emerging from the translating ribosome. SRP in *Escherichia coli* is composed of one protein, Ffh, and 4.5 S RNA. In the present work, we probe the structure of Ffh alone and in the complex with 4.5 S RNA by measuring distances between different positions within Ffh and between Ffh and 4.5 S RNA by fluorescence resonance energy transfer (FRET). According to the FRET distances, NG and M domains in free Ffh are in close contact, as in the A/A arrangement in the crystal structure of Ffh from *Thermus aquaticus*, in agreement with the formation of a crosslink between cysteine residues at two critical positions in the G and M domains. Upon Ffh binding to 4.5 S RNA or a 61 nucleotide fragment comprising internal loops A–C, the G and M domains move apart to assume a more open conformation, as indicated by changes of FRET distances. The movement is smaller when Ffh binds to a 49 nucleotide fragment of 4.5 S RNA comprising only internal loops A and B, i.e. lacking the binding site of the NG domain. The FRET results suggest that in the SRP complex 4.5 S RNA is present in a bent, rather than extended, conformation. The domain rearrangement of Ffh that takes place upon formation of the SRP is probably important for subsequent steps of membrane targeting, including interactions with the translating ribosome and the SRP receptor.

Keywords: protein targeting; fluorescence anisotropy; fluorescence lifetime; FRET; bimane crosslink

Introduction

Targeting of proteins, including the insertion and translocation of proteins into or across membranes, is a fundamental process in cells, and a variety of specialized mechanisms for protein transport have developed during evolution. The signal recognition particle (SRP) is found in the cytoplasm of eukaryotes and prokaryotes, where it plays a central role in the co-translational targeting of ribosomes translating export or membrane proteins to the membrane of the endoplasmic reticulum and the plasma membrane, respectively.[1–3]

Bacterial SRP consists of protein Ffh and 4.5 S RNA. Ffh (SRP54 in eukaryotes) is the only protein that is conserved in SRP from all organisms;[4] Ffh is essential for signal peptide binding,[5,6] and for complex formation with the SRP receptor,[7] and with the ribosome.[8] Ffh consists of three domains: the N-terminal four-helix bundle (N domain), the central GTPase domain (G domain) and the methionine-rich C-terminal domain (M domain).[9] The N and G domains are packed tightly against each other, forming a structural and functional unit, the NG domain, although there seems to be some mobility between N and G domains.[10] Crystal structures of the NG domain of Ffh from bacteria and SRP54 from archaea[11–13] have been reported. The structures of the N and G domains in full-length Ffh are very similar to the structure of the

Abbreviations used: SRP, signal recognition particle; FRET, fluorescence resonance energy transfer; dBrB, dibromobimane; mBrB, monobromobimane; OG, Oregon green 488; Bpy, BODIPY FL; Alx555, Alexa Fluor 555; Alx647, Alexa Fluor 647.

E-mail address of the corresponding author: winterme@uni-wh.de

NG fragment solved at 1.1 Å resolution.[9,11] The structure of a major part of the M domain with and without bound SRP RNA has been determined for *Escherichia coli* Ffh, human SRP54, and Ffh from *Thermus aquaticus*.[9,14–16] The M domain is an α-helical domain featuring a prominent hydrophobic cleft and an extended flexible "finger" loop.[9] Adjacent to the cleft, helices 3 and 4 form a helix-turn-helix motif that confers high-affinity binding to SRP RNA.[17]

As the linker region between the G and M domains, including the N-terminal part of the M domain, was not ordered in most structures, except that of SRP54 from *Sulfolobus solfataricus*,[18] there is no consistent information on the domain arrangement in Ffh or the Ffh–4.5 S RNA complex. On the basis of the crystal structures available so far, several different domain arrangements of Ffh seem to be possible. From the positions of NG and M domains in the crystal of Ffh trimer,[9] two arrangements (A/A, i.e. A chain representing both NG and M domains; or B/A, B chain for NG and A chain for M; Figure 1(a)) are compatible with the length of the linker and may therefore represent the solution structure of Ffh.[9] A different domain arrangement was found in the crystal structure of SRP54 from *S. solfataricus* determined at ~4 Å resolution.[18] In that structure (Figure 1(a)), the protein is present in an open, L-shaped conformation and the interaction between Ffh domains is limited to a hydrophobic contact between the N and M domains, while the G domain is about 30 Å away from the M domain. In the complex of *S. solfataricus* SRP54 with a 49 nt 4.5 S RNA fragment, the NG domain is shifted slightly further away from the M domain by a rotation of the domains relative to each other.[18]

The 4.5 S RNA is a 114 nt molecule that contains a conserved apical tetraloop and a number of internal loops (loops A–E) connected by short double helices.[19,20] The structure of full-length 4.5 S RNA is not known. Secondary structure predictions based on thermodynamic stability and evolutionary conservation indicated a highly base-paired, rod-like structure.[19,21,22] However, fluorescence, melting and chemical modification studies suggested the possibility of an alternative, bent conformation of the RNA.[23,24] In SRP, the M domain of Ffh binds to loops A and B of 4.5 S RNA, and protects this region from chemical modification and enzymatic cleavage.[15,18] The crystal structure (at 1.8 Å resolution) of the *E. coli* Ffh M domain bound to a 49 nt fragment of 4.5 S RNA revealed that helices 3 and 4 of the M domain bind the distorted minor groove of the RNA and are recognized by C62 and

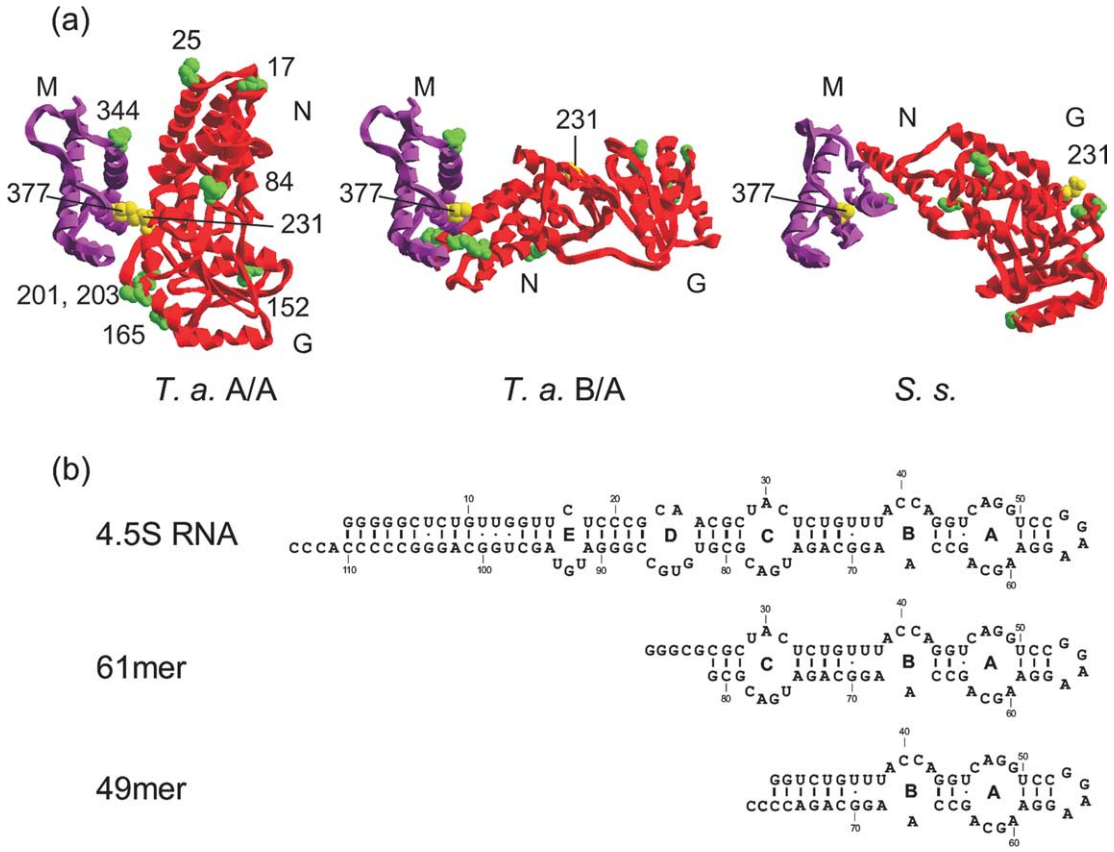

Figure 1. Ffh structures and 4.5 S RNA constructs. (a) Domain arrangements in the crystal structures of trimeric *T. aquaticus* (T.a.) Ffh[9] in A/A and B/A configuration of NG and M domains and of *S. solfataricus* (S.s.) SRP54.[18] The N, G, and M domains are indicated. Positions at which fluorescence dyes were introduced at cysteine residues are indicated in green; Cys231 and Cys377 that were crosslinked by dBrB are indicated in yellow. (b) The 4.5 S RNA constructs used in the present work.

A47 in loop A of 4.5 S RNA.[15] In the complex with full-size SRP, Ffh protects residues in loops A through D from chemical modification and enzymatic cleavage;[24] protection in loops A and B is due to binding of the M domain,[15,25] whereas protection in loop C reflects binding of the NG-domain of Ffh.[25] Crosslinking studies suggest that 4.5 S RNA in SRP may be present in a bent conformation with two potential pivot points at internal loop C,[20] and internal loop E.[26]

The aim of the present work was to study the domain arrangement of Ffh alone and in the complex with 4.5 S RNA, as well as the conformation of 4.5 S RNA in SRP. We introduced fluorescence reporter groups at a number of cysteine residues engineered into non-conserved surface positions of the NG and M domains. Fluorescence resonance energy transfer (FRET) within free Ffh was measured between identical fluorophores, and the respective distances were calculated from the FRET efficiency. On the basis of crystal structures and FRET distances, we identified two positions in the NG and M domains that were predicted to be close enough to be crosslinked; cysteine residues were introduced at the two positions and crosslinked by the thiol-specific bifunctional crosslinker dibromobimane (dBrB). The distances between different positions in SRP were determined from FRET between identical dyes in Ffh or different dyes attached to Ffh and three positions in 4.5 S RNA. The data, in conjunction with crystal structures of isolated Ffh domains,[9,15] and 4.5 S RNA structural models,[20,26] were used to build structural models of free Ffh and SRP, respectively.

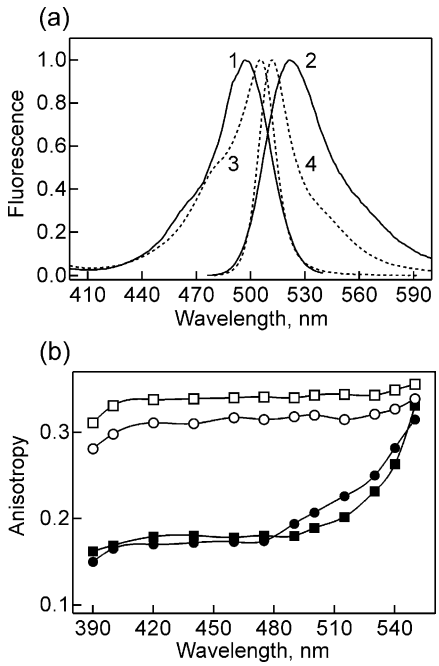

Figure 2. FRET between two identical fluorophores. (a) Normalized excitation (1, 3) and emission (2, 4) spectra of Oregon green 488 (1, 2) and Bodipy-FL (3, 4) attached to Ffh at position 165. (b) Excitation anisotropy spectra. Double-labeled Ffh(OG84/344) (filled circles), equimolar mixture of single-labeled Ffh(OG84) and Ffh(OG344) (open circles), double-labeled Ffh(Bpy203/344) (filled squares), equimolar mixture of single-labeled Ffh(Bpy203) and Ffh(Bpy344) (open squares). Measurements were performed at 20 °C in buffer A containing 90% (v/v) glycerol.

Results

Domain arrangement in free Ffh

A number of Ffh mutants were constructed with one or two cysteine residues at non-conserved surface positions. In the NG domain, cysteine residues were introduced in positions 17, 25, 84, 152, 165, 201, or 203 (Figure 1(a)). In the M domain, the intrinsic cysteine residue at position 406 was replaced with serine, while cysteine was introduced at position 344. The cysteine residues were labeled with either Oregon green 488 (OG) or BODIPY FL (Bpy) for measuring FRET between either two OG or two Bpy fluorophores. OG and Bpy are particularly well suited for measuring FRET between two identical fluorophores, because of the extensive overlap between their excitation and emission spectra (Figure 2(a)); the protein-bound fluorophores exhibit $R_{0(2/3)}$ values (50% FRET efficiency) of 43 Å (OG-OG) and 54 Å (Bpy-Bpy). When the two fluorophores are sufficiently close to each other, the fluorescence anisotropy is lowered as a result of FRET.[27] In order to determine FRET efficiencies, fluorescence anisotropies were measured for the double-labeled proteins and compared to the anisotropies of the equimolar mixtures of the respective single-labeled proteins (Table 1). For single-labeled Ffh, the anisotropies of both OG and Bpy attached to any position of the protein were high, 0.31–0.33, indicating low mobility of the labels. In all cases, the anisotropy values were lowered when the second dye was present, yielding FRET efficiencies between 33% and close to 100% (Table 1).

That the decrease of the anisotropies in double-labeled Ffh was due to FRET was verified by varying the excitation wavelength (Figure 2(b)). The effect of FRET on the observed anisotropy is expected to be diminished when the excitation wavelength is shifted to the red, because the overlap of excitation and emission spectra becomes smaller upon excitation at longer wavelengths due to a red shift of the emission spectrum caused by solvent orientation effects (the "red-edge effect").[28] Shifting the excitation to longer wavelengths increased the anisotropy of double-labeled Ffh up to the level of the single-labeled controls, whereas the anisotropies of single-labeled Ffh remained unaffected, demonstrating that the lower anisotropy values observed for double-labeled Ffh were due to FRET.

Table 1. Distances between identical fluorophores attached to position 344 in the M domain and various positions in the NG domain of *E. coli* Ffh determined by fluorescence anisotropy

		Anisotropy				Distance in crystal structure		
Probe (Å)[a]	Position	r_{Di}[b]	r_{DD}[c]	E[d]	R (Å)[e]	*T.a.* A/A	*T.a.*B/A	*S.s.*
OG	17	0.319	0.188	0.81	34	33	34	22
	25	0.311	0.163	0.96	<27[f]	27	47	31
	84	0.310	0.160	0.98	<27[f]	24	52	24
	152	0.314	0.259	0.35	48	48	62	47
	165	0.312	0.261	0.33	48	49	78	57
	201	0.317	0.210	0.66	38	37	66	50
	203	0.317	0.212	0.66	39	37	73	52
	344	0.315						
Bpy	152	0.322	0.205	0.70	47	48	62	47
	165	0.332	0.211	0.68	48	49	78	57
	201	0.321	0.174	0.90	38	37	66	50
	203	0.323	0.175	0.89	38	37	73	52
	344	0.309						

[a] Distances from the given position to position 344 in the A/A and B/A arrangements of the *T. aquaticus* Ffh trimer (*T.a.* A/A and B/A, respectively)[9] or in *S. solfataricus* SRP54 (*S.s.*).[18] Distances were measured between sulfur atoms of cysteine residues at the respective positions using RasMol.

[b] r_{Di}, limiting anisotropy of the dye attached to a single position of Ffh.

[c] r_{DD}, anisotropy of the ensemble of two dyes attached to position 344 and to one of the other positions.

[d] E, FRET efficiency, calculated from anisotropy differences observed in the presence of one (r_{Di}) or two (r_{DD}) fluorophores (Materials and Methods). Values are for buffer A containing 90% (v/v) glycerol; within 2 Å the same respective distances were obtained in buffer A contaning 20% or 60% (v/v) glycerol.

[e] The distance between two dyes, R, was calculated from the FRET efficiency (Materials and Methods). The uncertainty range of the distances, ±10 Å, was calculated using depolarization factors (Materials and Methods). The uncertainty is much larger than the error introduced by the standard deviation of the anisotropy measurement, 0.002.

[f] At FRET efficiencies >0.95, due to low precision of the measurement only upper limits of the distances, <27 Å, are given.

Distances between position 344 in the M domain and various positions in the N or G domains were calculated from FRET efficiencies (Table 1). For a given position, identical distances to C344 were obtained with OG and Bpy. Due to the limited rotational mobility of the dyes, as indicated by the high anisotropy values measured for single-labeled Ffh, the uncertainty ranges of the distances derived from FRET are relatively large, up to ±10 Å. Nevertheless, the discrimination of models derived from different crystal structures of Ffh or SRP54 was possible. All distances determined by FRET were consistent with those of the A/A configuration of NG and M domains in the crystal structure of Ffh from *T. aquaticus*.[9] The FRET distances between position 344 and positions 25, 84, 165, 201, or 203 were not consistent with the B/A orientation.[9] Two positions, 165 and 201, were significantly further away from position 344 in *S. solfataricus* SRP54 than measured by FRET,[18] whereas position 17 appeared to be closer to 344 in the crystal than in solution. These results suggest that the orientation of NG and M domains in free Ffh from *E. coli* corresponds to the A/A configuration in the crystal of *T. aquaticus* Ffh,[9] rather than to the B/A configuration,[9] or to the open domain arrangement in the crystal structure of SRP54 from *S. solfataricus*.[18]

Discrimination of domain orientations by dibromobimane crosslinking

The FRET distances within Ffh in conjunction with the crystal structure suggested two residues in the G domain (residue 231) and M domain (residue 377) that are predicted to be close to one another in the A/A configuration, but far apart in all alternative configurations (Figure 1(a)).[9] To test whether the two positions are in fact adjacent, we introduced cysteine residues at both positions and crosslinked them with the bifunctional crosslinker dBrB, which reacts specifically with thiol groups and can crosslink pairs of thiol groups within 3–6 Å of one another (Figure 3(a)).[29] The feasibility of dBrB crosslinking of the double-cysteine mutant, Ffh(C231/377), has been demonstrated,[25] and the reaction and the crosslinking product are analyzed here in more detail. The crosslinking reaction can be monitored by fluorescence, because dBrB becomes fluorescent when the two bromine atoms, which are strong quenchers of fluorescence, are released during the reaction. The reaction of Ffh(C231/377) with dBrB in fact led to a fluorescence increase that was completed after one hour, indicating the formation of the crosslink (Figure 3(b)). Control reactions were performed with monobromobimane (mBrB), which becomes fluorescent upon coupling to a single thiol group, and the respective single-cysteine mutants, Ffh(C231) and Ffh(C377). Compared to the reaction with dBrB, the control reactions followed similar time-courses and led to comparable fluorescence levels, indicating that the formation of the crosslink did not require a significant distortion of the protein and that cysteine residues 231 and 377 were close to one another in the native conformation of the protein. Crosslink formation was not observed in SRP(C231/377), indicating that the two positions move apart upon Ffh binding to 4.5 S RNA (see

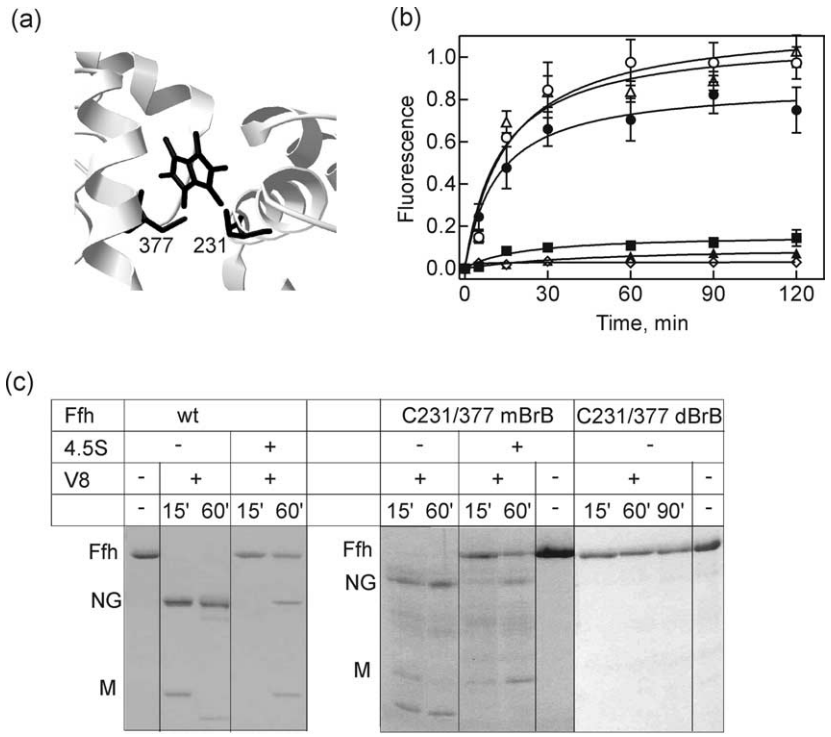

Figure 3. Bimane crosslinking of G and M domains of Ffh. (a) Model of bimane crosslinked to Ffh(C231/377). The structure of *T. aquaticus* Ffh in the A/A orientation was used (PDB accession number 2FFH),[9] in which the residues corresponding to positions 231 and 377 in *E. coli* Ffh (228 and 363 in *T. aquaticus*, respectively) were replaced with cysteine residues using RasMol software. (b) Reaction of dibromobimane (dBrB) and monobromobimane (mBrB) with cysteine mutants of Ffh. The time-course of the reaction was followed by monitoring bimane fluorescence. Relative amounts of Ffh were determined by SDS-PAGE. Ffh(C231/377)/dBrB (filled circles); Ffh(C231)/mBrB (open circles); Ffh(C377)/mBrB (open triangles); SRP(C231/377)/dBrB (filled squares); Ffh(C406S)/dBrB (open diamond); Ffh(C17/344)/dBrB (filled triangles). (c) V8 protease digestion of bimane-crosslinked Ffh. Digestions with V8 protease were performed and the digestion mixtures analyzed by SDS-PAGE as described in Materials and Methods.[30] The positions of intact Ffh, NG domain, and M domain are indicated.

below).[25] Another double-cysteine mutant, Ffh(C17/344), did not yield a fluorescent product with dBrB, i.e. no crosslink, consistent with the large distance between those two cysteine residues. The mobility in SDS/polyacrylamide gels of bimane-crosslinked Ffh was the same as that of unmodified Ffh (Figure 3(c)), confirming that the crosslink was intramolecular, rather than intermolecular.

The formation of the bimane crosslink in Ffh, which connects G and M domains, was verified by proteolysis with V8 protease, which preferentially cleaves the linker connecting M and G domains and, upon prolonged incubation, within the M domain (Figure 3(c)).[30] In the Ffh complex with 4.5 S RNA, both cleavages are inhibited.[30] Cysteine insertion and bimane modification as such did not impair proteolysis, as very similar cleavage patterns were observed for wild-type Ffh and Ffh(C231/377) modified by mBrB. Upon V8 cleavage of bimane-crosslinked Ffh, however, there was no separation of NG and M domains on SDS-PAGE, despite the cleavage in the linker region, indicating that the two domains were held together by the crosslink. In keeping with the FRET measurements, this result strongly favors a model in which NG and M domains are aligned closely, as in the A/A domain arrangement in free Ffh.[9]

Orientation of Ffh domains in SRP

In order to assess conformational changes induced in Ffh upon binding to 4.5 S RNA, FRET measurements were performed on Ffh–RNA complexes to determine distances within Ffh and from various positions in Ffh to the 3′ ends of 4.5 S RNA and fragments of 4.5 S RNA. First, changes of distances between different positions in Ffh caused by binding to 4.5 S RNA were determined from efficiencies of FRET between two identical fluorophores (OG or Bpy) attached to Ffh as described above, again measuring fluorescence anisotropies. Three different 4.5 S RNA constructs were used (Figure 1(b)): full-length 4.5 S RNA, truncated 4.5 S RNA comprising internal loops A–C (61mer, residues 21 to 81), and a 49 nt fragment that comprised internal loops A and B and an extended double-stranded stem replacing loop C (49mer);[15] the latter fragment was used because crystal structures of its complexes with the M domain[15] or full-size SRP54 are available.[18] The fluorescence anisotropy of double-labeled Ffh was compared to that of an equimolar mixture of the respective single-labeled species, and FRET efficiencies and distances were calculated from the difference, as described above for free Ffh. Upon binding to full-size 4.5 S RNA or the 61mer fragment, several distances in Ffh changed significantly (Table 2), indicating a conformational change of Ffh. The distances between the G domain (positions 165, 201, and 203) and the M domain (position 344) increased, suggesting that the domains moved apart. Also, position 84 at the interface between the N and G domains showed a tendency to move away from the M domain, although, given the uncertainty margins of the distances, this change

Table 2. Distances between fluorophores attached to position 344 in the M domain and various positions in the NG domain of Ffh bound to truncated or full-length 4.5 S RNA

	R (Å)[a]				Distance (Å) in Ffh
Position[b]	Free Ffh	49mer	61mer	4.5 S RNA	*S.s.* SRP54-49mer[c]
17^{OG}	34	<27[d]	<27[d]	30	17
25^{OG}	<27[d]	<27[d]	31	32	30
84^{OG}	<27[d]	<27[d]	41	40	25
$152^{OG,Bpy}$	48	55	62	58	48
$165^{OG,Bpy}$	48	61	68	73	65
201^{Bpy}	38	51	64	64	52
203^{Bpy}	39	53	63	64	55

[a] Distances, R, were calculated from FRET efficiencies as in Table 1. Uncertainty ranges of ±10 Å were calculated from depolarization factors (Materials and Methods). 49mer, 61mer, 4.5 S RNA: distances between position 344 and the indicated position in Ffh bound to the respective RNA. Distances for free Ffh from Table 1.
[b] OG or Bpy at the indicated position in the NG domain and at position 344 in the M domain.
[c] Distances from the crystal structure of the complex of *S. solfataricus* SRP54 with the 49mer.[18]
[d] Precise calculation is not possible due to very high transfer efficiency (>95%); cf. Table 1.

was close to the uncertainty range. Positions 17, 25, and probably also 152, did not change their positions significantly relative to position 344.

The conformational rearrangements that would account for the observed distances in SRP, as compared to free Ffh, indicate a rotation of the NG domain by about 40° around a pivot at residue 84, resulting in a movement of the G domain from the A/A orientation away from the M domain into a more open configuration, while the N domain moves slightly towards the M domain. The binding of the 49mer RNA fragment to Ffh caused a somewhat smaller conformational change, as the G domain moved less than upon interaction with full-size 4.5 S RNA or the 61mer. The distances within Ffh in the complex with the 49mer are consistent with those in *S. solfataricus* SRP54 bound to the same RNA fragment,[18] except at position 25, where the efficiency of FRET was too high to allow for a reliable distance determination, suggesting that this group was very close to residue 344 in the M domain. Thus, the two domain orientations, the opened A/A arrangement and that found in *S. solfataricus* SRP, cannot be distinguished by FRET measurements with the labels within Ffh.

For further analysis, we measured FRET between one fluorophore (OG or Bpy) attached to Ffh as donor and another (Alexa Fluor 555 or 647, Alx) attached to the 3′ end of full-length or truncated 4.5 S RNA as acceptor. Due to different overlap integrals (Figure 4(a); Materials and Methods), the three different donor–acceptor couples used covered an extended distance range, with $R_{0(2/3)}$ values (50% FRET efficiency) of 66 Å (OG/Alx555), 50 Å (OG/Alx647), and 44 Å (Bpy/Alx647). FRET efficiency was measured by comparing the fluorescence of Ffh–RNA complexes in which only Ffh was labeled (donor alone) with that of the complexes of labeled Ffh with labeled RNA (donor plus acceptor). Examples are shown in Figure 4(b), (c), and (d) for the 49mer, 61mer, and full-length 4.5 S RNA, respectively. In addition, fluorescence lifetimes of the donor were measured in the absence and in the presence of acceptor, and the FRET efficiency was determined from the lifetime change; fluorescence lifetimes for Ffh complexes with 49mer and 61mer were measured by the time domain method (examples in Figure 4(e)); for the complexes with full-length 4.5 S RNA, the frequency domain method was employed (Figure 4(f)). All results and the respective distances calculated from FRET efficiencies are summarized in Tables 3–5. Essentially identical distances were obtained when different donor–acceptor pairs were compared.

In the Ffh–49mer complex, position 344 in the M domain was 68(±5) Å away from the 3′ end of the 49mer. This distance is in good agreement with 63 Å measured in a model of the 49mer-M domain complex obtained by superposition of the M domain of isolated Ffh[9] with the 49mer-M domain crystal structure (the finger loop encompassing position 344 is missing from the crystal structure),[15] but is significantly larger than that predicted from the structure of the *S. solfataricus* SRP54–49mer complex, which is about 50 Å.[18] According to the FRET measurements, positions 165, 201, and 203 in the G domain were within 35 Å from the 3′ end of the 49mer, whereas positions 17 and 25 in the N domain were about 70–80 Å away. Comparing these distances with those measured in the *S. solfataricus* SRP54–49mer complex indicated that several distances are incompatible with the FRET measurement, in particular those involving positions 165, 201, and 203 (Table 3).[18] Rather, the measured distances are consistent with a model obtained by moving apart the NG and M domains of the A/A structure in the Ffh trimer,[9] in order to accommodate RNA and avoid steric clashes (Figure 5(b)). This model accounts for the FRET distances measured within Ffh (Table 2) and from the 3′ end of the 49mer to all positions in Ffh (Table 3) within the respective uncertainty ranges.

Conformation of 4.5 S RNA in SRP

The 49mer fragment does not comprise the complete binding site of Ffh, because it lacks the

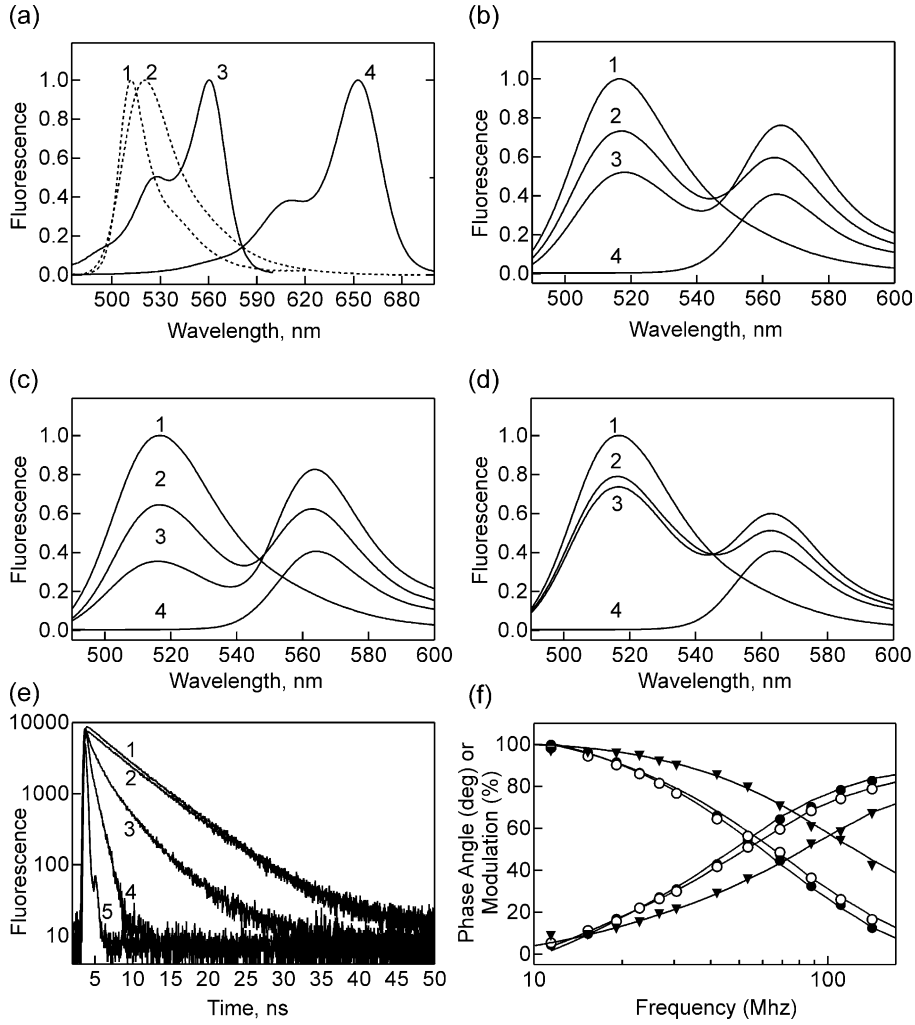

Figure 4. FRET between Ffh and the 3′ end of truncated and full-length 4.5 S RNA measured by steady-state and time-resolved fluorescence. (a) Spectral overlap characteristics. Normalized corrected fluorescence emission spectra of Oregon green 488 (1) and Bodipy-FL (2) attached to Ffh (position 25 or 344) and excitation spectra of Alexa Fluor 555 (3) and Alexa Fluor 647 (4) attached to 3′-end of 4.5 S RNA. Spectra of OG/Bpy-labeled Ffh bound to the 49mer were the same as spectra (1) and (2), respectively. (b) Emission spectra of Ffh(OG25)–49mer or Ffh(OG344)–49mer (1), Ffh(OG25)–49mer(Alx555) (2); Ffh(OG344)–49mer(Alx555) (3), Ffh–49mer(Alx555) (4). (c) Emission spectra of Ffh(OG25)–61mer or Ffh(OG344)–61mer (1), Ffh(OG25)–61mer(Alx555) (2); Ffh(OG344)–61mer(Alx555) (3), Ffh–61mer(Alx555) (4). (d) Emission spectra of Ffh(OG25)–4.5 S RNA or Ffh(OG344)–4.5 S RNA (1), Ffh(OG25)–4.5 S RNA(Alx555) (2), Ffh(OG344)–4.5 S RNA(Alx555) (3), Ffh–4.5 S RNA(Alx555) (4). (e) Time-domain lifetime measurements. Ffh(OG152) plus: 4.5 S RNA (1), 4.5 S RNA(Alx555) (2), 49mer(Alx555) (3), 61mer(Alx555) (4); the excitation pulse is also shown (5). For the evaluation of the decay curves by single-exponential or multi-exponential fitting, see Materials and Methods. Average lifetimes resulting from the fits are given in Tables 3–5. (f) Frequency-domain lifetime measurements. Ffh(OG25) (open circles) plus: 4.5 S RNA (filled circles), 4.5 S RNA(Alx555) (triangles). Increasing curves, phase angles; decreasing curves, modulation. For evaluation, see Materials and Methods.

internal loop C to which the NG domain binds,[25] suggesting that the Ffh–49mer complex may not be representative for SRP. Thus, the conformation of Ffh in SRP was derived from the FRET distances measured in the complexes with the 61mer fragment and 4.5 S RNA. Binding of the 61mer to Ffh resulted in very strong FRET between the label at the 3′ end of the fragment and positions 152, 165, 201, and 203 in the G domain, indicating close proximity, and intermediate FRET to position 344, corresponding to a distance of 61 Å (Table 4). The attempt to build a model of SRP using the opened variant of the A/A domain arrangement of Ffh described above for the Ffh–49mer complex and an extended structure of the 61mer provided no satisfactory solution that would accommodate FRET distances measured both within Ffh (Table 2) and between Ffh and the 61mer 3′ end (Table 4), because the 3′ end of the extended 61mer was too far away from all positions mentioned above. However, the observed distances could be explained easily by using a model in which 4.5 S RNA was bent at the asymmetric loop C (Figure 5(c)).[20]

Table 3. Distances between the 3′ end of the 49mer fragment of 4.5 S RNA and various positions in Ffh as determined by steady-state and time-resolved FRET

Probes[a]	Position in Ffh	F_{DA}/F_D	τ_D (ns)	τ_{DA} (ns)	E[b]	R[c] (Å)	$S.s.$[d] (Å)	Δ[e] (Å)
OG/Alx555	17	0.62	4.1	2.6	0.37	72	65	−7
	25	0.74	4.1	3.0	0.27	79	76	−3
	344	0.55	4.1	2.3	0.45	69	50	−19
OG/Alx647	84	0.79	4.1	3.4	0.19	64	59	−5
	152	0.35	4.0	1.5	0.64	46	38	−8
	165	0.18	4.1	0.7	0.82	39	54	+15
Bpy/Alx647	152	0.41	5.0	1.9	0.60	41	38	−3
	165	0.17	5.1	0.7	0.84	33	54	+21
	201	0.15	5.1	0.8	0.84	33	67	+34
	203	0.14	5.1	0.8	0.85	33	65	+32
	344	0.91	5.1	4.8	0.08	67	50	−17

[a] OG or Bpy were attached to the indicated positions in Ffh, Alx555 or Alx647 to the 3′ end of the 49mer.
[b] Transfer efficiencies, E, were calculated from both fluorescence intensities and lifetimes (Materials and Methods). Comparable values (within 5%) were obtained from the two measurements and mean values are given. Distances, R, were calculated from E (Materials and Methods).
[c] The relatively small uncertainty range of ±5 Å, as determined from depolarization factors, resulted from the high mobility (limiting anisotropy <0.15) of Alx555/Alx647 at the 3′ end of the RNAs (Materials and Methods).
[d] Distance taken from the crystal structure of *S. solfataricus* SRP54 in the complex with the 49mer fragment.[18]
[e] *S.s.* distances minus FRET distances.

Furthermore, based on frequency-domain FRET measurements (Figure 4(f); Table 5) we found FRET from several positions in Ffh to the 3′ end of full-length 4.5 S RNA; yielding distances in the range of 80–90 Å (Table 5); from positions 152 and 165 no significant FRET was observed. Positions 201 and 203 could not be examined, because OG at these positions interfered with formation of the Ffh–4.5 S RNA complex. The distances predicted from placing a fully extended 4.5 S RNA into the SRP model are >100 Å for all Ffh positions. Furthermore, also in a model with one bend at loop C and the rest of the molecule extended, the 3′ end of 4.5 S RNA is >100 Å away from all four positions in Ffh exhibiting efficient FRET (Figure 6). However, when a second bend was introduced in loop E of 4.5 S RNA, the model was consistent with the FRET distances (Table 5; Figure 6). A bend at loop D is considered unlikely, because it results in serious clashes within the RNA.

Discussion

The present FRET measurements suggest that the domain arrangement in free *E. coli* Ffh is represented by the first molecule (A/A) of the asymmetric unit in the crystal structure of *T. aquaticus* Ffh.[9] This arrangement is supported strongly by the results of dBrB crosslinking, which show that positions 231 (G domain) and 377 (M domain) of Ffh are located within 3–6 Å of each other. The arrangement derived from FRET and crosslinking is incompatible with the two other domain arrangements in the trimer (B/A, C/A) and the arrangement present in the crystal structure of SRP54 from *S. solfataricus*.[18]

The present FRET measurements show that binding of 4.5 S RNA results in a movement of the G domain away from the M domain, while the N domain comes closer to the M domain, opening a cleft between M and NG domains that accommodates

Table 4. Distances between the 3′ end of the 61mer fragment of 4.5 S RNA and various positions in Ffh as determined by steady-state and time-resolved FRET

Probe[a]	Position in Ffh	F_{DA}/F_D	τ_D (ns)	τ_{DA} (ns)	E[b]	R[c] (Å)
OG/Alx555	17	0.68	4.1	2.7	0.32	68
	25	0.67	4.1	2.7	0.33	70
	344	0.38	4.1	1.5	0.62	61
OG/Alx647	84	0.69	4.1	2.1	0.40	53
	152	0.04	4.0	<0.5	0.96	<30
Bpy/Alx647	152	0.05	5.1	<0.5	0.95	<25
	165	0.02	5.1	<0.5	0.98	<25
	201	0.01	5.1	<0.5	0.99	<25
	203	0.01	5.1	<0.5	0.99	<25
	344	0.92	5.0	4.6	0.08	61

[a] OG or Bpy were attached to different positions in Ffh, Alx555 or Alx647 to the 3′ end of the 61mer.
[b] For the determination of FRET efficiencies and distances, see Table 3. For positions where the lifetime of the donor was reduced to <0.5 ns and the FRET efficiency was >95%, upper limits for the distances are given, taking into account the different R_0 values.
[c] Uncertainty range of distances ±5 Å (see Table 3).

Table 5. Distances between the 3′ end of 4.5 S RNA and various positions in Ffh as determined by steady-state and time-resolved FRET

Probes[a]	Position	F_{DA}/F_D	τ_D (ns)	τ_{DA} (ns)	E[b]	R[c] (Å)	Predicted (Å) bent/straight[d]
OG/Alx555	17	0.82	4.1	3.4	0.17	85	83/133
	25	0.76	4.1	3.2	0.24	81	73/121
	84	0.80	4.0	3.5	0.16	90	85/124
	152	1.00	nd	nd	0	>90	108/125
	165	1.00	nd	nd	0	>90	105/113
	344	0.75	4.0	3.1	0.23	82	63/114

nd, not determined.
[a] OG was attached to various positions in Ffh and Alx555 to the 3′ end of 4.5 S RNA.
[b] For the determination of FRET efficiencies and distances, see Table 3.
[c] Uncertainty range of distances ±5 Å (see Table 3).
[d] Models with bent or straight loop E of 4.5 S RNA (Figure 6).

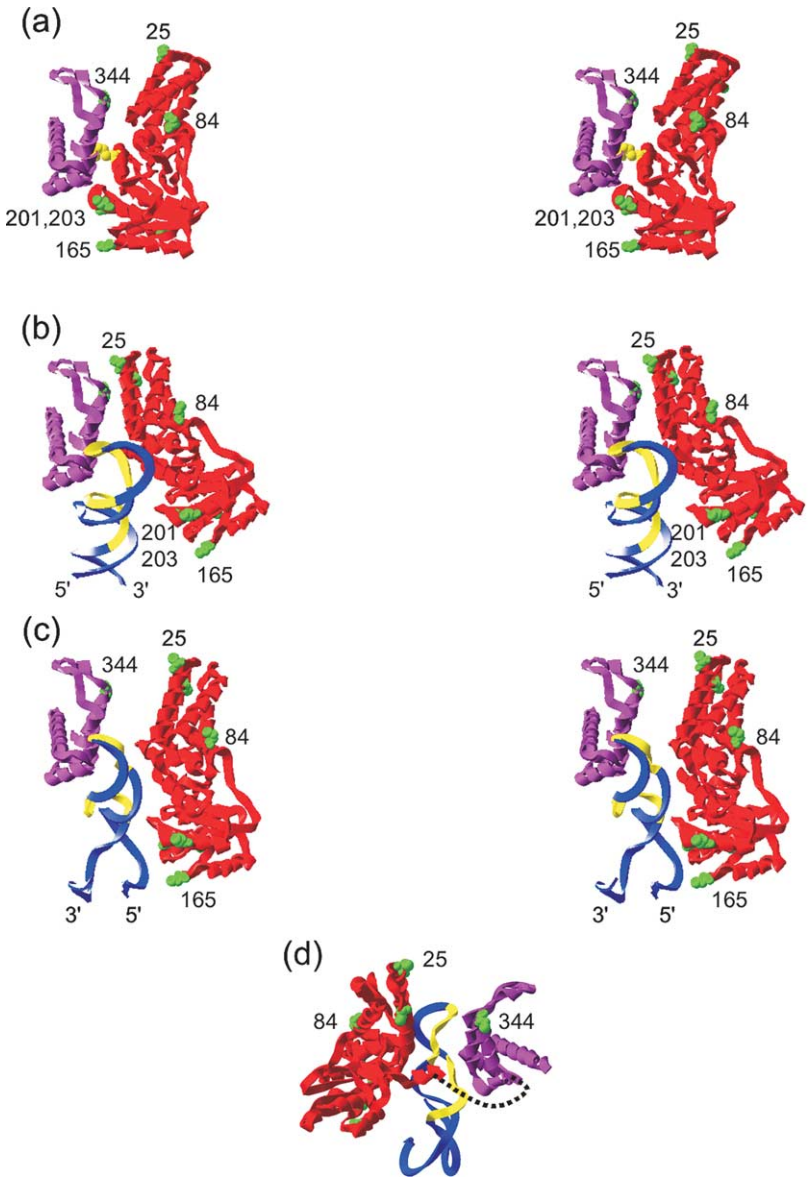

Figure 5. Structural models of free Ffh, the Ffh–49mer complex and the Ffh–61mer complex. (a) Stereo model of Ffh. The M (purple) and NG (red) domains are arranged in the A/A configuration of the crystal structure of *T. aquaticus* Ffh.[9] Cysteine residues where OG or Bpy were attached are labeled green and numbered (for complete numbering, see Figure 1(a)). Cysteine residues 231 and 377 crosslinked by bimane are colored yellow. The arrangement of NG and M domains fits all FRET distances (Table 1) within ±5 Å. (b) Stereo model of the Ffh–49mer complex. The 49mer–M domain arrangement is taken from the crystal structure of the complex.[15] The 49mer is colored blue and regions protected by Ffh against chemical modification are colored yellow.[24] (c) Stereo model of the Ffh–61mer complex; coloring as in (b). The model of the RNA, including a 50° kink at internal loop C, was taken from Gorodkin *et al.*[20] (d) Alternative view of the Ffh–61mer model. The model shown in (c) was turned by 180° and tilted slightly to show the presumed path of the linker (dotted line) connecting positions 307 (G domain) and 319 (M domain).

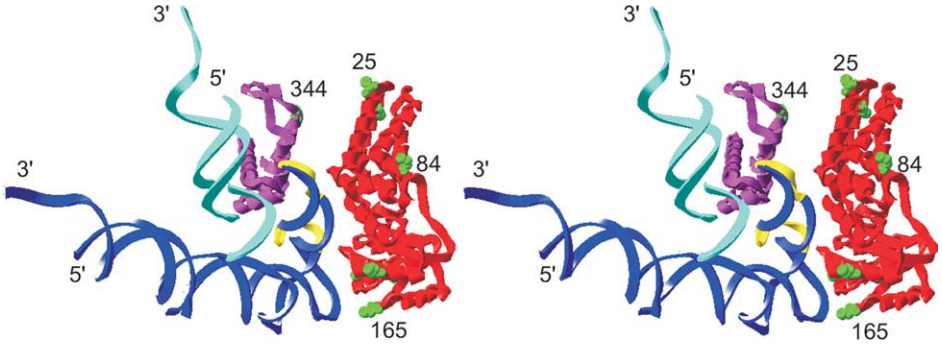

Figure 6. Stereo model of the Ffh–4.5 S RNA complex. Based on the structural model of the Ffh–61mer complex with the RNA bent at loop C (Figure 5(c)), full-length 4.5 S RNA was modeled with loop E straight (dark blue) or bent by 120° (light blue). The distance between the 3′ end of the RNA and position 344 in the M domain is shorter in the model (63 Å) than measured by FRET (82 Å) in order to account for an observed crosslink from the 5′ end of 4.5 S RNA and Ffh.[26]

the RNA. Footprinting and biochemical studies indicated that both M and NG domains interact with 4.5 S RNA,[25] the M domain interacting at loops A and B,[15] and the NG domain at loop C.[25] In the model of SRP (Figure 5), it is the G domain that interacts with the RNA and the linker between NG and M domains would be located close to (or in contact with) 4.5 S RNA, which could explain why 4.5 S RNA protected the linker region of Ffh from digestion by V8 protease.[30] Together, the contacts of the M domain known from the crystal structure, the binding of the NG domain at loop C, and interactions with the linker region predicted by the structural model (Figure 5(c) and (d)) account for essentially all footprints of Ffh on 4.5 S RNA reported previously.[24] The distances predicted from the crystal structure of *S. solfataricus* SRP are not in agreement with the distances measured by FRET for *E. coli* SRP,[18] suggesting that either the crystal structure does not reflect the solution structure of SRP or the conformation of the complex is different in *E. coli* and *S. solfataricus*.

The structure of the full-length 4.5 S RNA alone is not known; it may assume a fully extended, rod-like structure, or a more globular conformation bent at one (or more) asymmetric loops. The present data indicate that position 81 of 4.5 S RNA in SRP is close (20–30 Å) to the G domain. Recently, a crosslink was found from this position of 4.5 S RNA to Ffh, suggesting that the reactive group was within 10–15 Å (the crosslinking distance) of the protein.[26] This short distance in conjunction with the FRET distances measured within Ffh and from Ffh to 4.5 S RNA is incompatible with the extended structure of 4.5 S RNA, but can be reconciled easily with the conformation of 4.5 S RNA with a bend in the internal loop C. Furthermore, the FRET measurements indicate that the 3′ end of 4.5 S RNA is closer to Ffh than predicted by both the extended and the singly bent conformations of 4.5 S RNA, suggesting that 4.5 S RNA can assume an even more compact conformation with bends at both loops C and E or oscillate between straight and bent conformations. The existence of a bent conformation of 4.5 S RNA in SRP in which the 5′ and 3′ ends are close to Ffh is supported by a strong crosslink formed between a crosslinker at the 5′ end of 4.5 S RNA and Ffh,[26] and by an influence of Ffh on the fluorescence of a label at the 3′ end of the RNA.[23]

In conclusion, our results indicate that both Ffh and 4.5 S RNA are flexible, dynamic molecules that change their conformation significantly upon binding to each other. It is likely that interactions with other components of the SRP targeting pathway, FtsY, and the ribosome may change the conformation of Ffh and 4.5 S RNA as well. In the SRP structural model proposed here, 4.5 S RNA occupies the position of the NG domain of FtsY as predicted by the NG-NG heterodimer structure.[31,32] This suggests that the conformation of the complex must change further to remove the steric hindrance and allow the interaction between the NG domains of Ffh and FtsY. Likewise, the conformation of SRP on the ribosome is likely to be different from that in solution. In fact, a more opened domain arrangement of SRP54 is suggested by the cryo-electron microscopy model of ribosome-bound mammalian SRP,[33] and crosslinking and cryo-electron microscopy data indicate that 4.5 S RNA in SRP on the ribosome is present in an extended conformation.[8,33,34] The nature, timing, and regulation of these conformational rearrangements and their importance for SRP function are important questions for future research.

Materials and Methods

Materials

Buffer A was 25 mM Hepes (pH 7.5), 70 mM ammonium acetate, 30 mM potassium acetate, 7 mM magnesium acetate. Alexa Fluor 555/647 hydrazides, Oregon green 488 maleimide, BODIPY-FL maleimide, as well as mono- and dibromobimane were from Molecular Probes. Ni-NTA agarose was from Qiagen. All other chemicals were obtained from Sigma or Merck.

Preparation of 4.5 S RNA

Full-size 4.5 S RNA and 61mer were prepared by phage T7 RNA polymerase transcription. The respective templates were amplified by Pfu polymerase using two primers, one coding for the T7 RNA polymerase promotor and a second coding for the end of the RNA, and used in the transcription reaction without further purification. Transcription was carried out in 5 ml of 40 mM Tris–HCl (pH 7.5), 1 mM spermidine, 10 mM DTT, 0.05% (v/v) Tween-20, 8 mM $MgCl_2$ containing 1 mM GMP, 2 mM ATP, GTP, CTP, UTP, 5 μg/ml of amplified DNA template, 1600 units/ml of T7 RNA polymerase (Fermentas), and 32 units/ml of RNase inhibitior (Fermentas) for four hours at 37 °C. RNA was purified by chromatography on MonoQ (Pharmacia) using a linear gradient of 0–1 M LiCl in 10 mM Bis–Tris (pH 6.0), 10 mM $MgCl_2$, 1 mM EDTA. The 49 nt fragment of 4.5 S RNA containing nucleotides 32–74 of 4.5 S RNA and three additional base-pairs at the end of the molecule was purchased from Dharmacon.[15]

Plasmid construction, protein expression, and purification

To construct Ffh mutants with single and double cysteine substitutions, the single cysteine residue present at position 406 of native Ffh was first substituted with serine. Cysteine mutants were generated by PCR mutagenesis by the QuickChange method using Pfu polymerase (Promega). Mutations were generated in plasmid pET24-Ffh coding for Ffh extended by six histidine residues at the C terminus and confirmed by DNA sequencing. Introducing cysteine residues and fluorescent dyes at any position used in this work did not affect the ability of Ffh to bind 4.5 S RNA, FtsY, or the ribosome (data not shown).[8,26]

Ffh mutants were expressed in *E. coli* BL21(DE3)pLysS cells and purified on Ni-NTA agarose under non-denaturing conditions: 10 g of cell pellet were resuspended in 40 ml of 20 mM Hepes (pH 7.5), 300 mM NaCl, 0.1 mM EDTA, 0.1 mM Pefablock SC (Roche) and 10 mM 2-mercaptoethanol, and the cells were opened by sonication (Branson Sonifier, duty cycle 50%, output 4) three times for five minutes on ice. The extract was centrifuged at 20,000*g* for 30 minutes. The supernatant was incubated with 5 ml of Ni-NTA agarose, equilibrated with 20 mM Hepes (pH 7.5), 300 mM KCl, 10 mM 2-mercaptoethanol, on ice for 60 minutes with shaking. The resin was washed with 150 ml of 20 mM Hepes (pH 7.5), 1 M KCl, 10 mM imidazole, 10 mM 2-mercaptoethanol, and Ffh was eluted with 20 ml of 20 mM Hepes (pH 7.5), 300 mM KCl, 250 mM imidazole, 20% (v/v) glycerol. The protein was further purified by gel-filtration on a Superdex 75 column (Pharmacia) in buffer A with 10% (v/v) glycerol. The concentration of glycerol was adjusted to 50% (v/v), and protein was concentrated by ultrafiltration using 30 kDa (NG domain, full-size Ffh) or 5 kDa (M domain) cut-off membranes (Vivaspin) at 4 °C. The purity of proteins was more than 95% according to SDS-PAGE. FtsY(W342) was expressed in *E. coli* BL21(DE3)pLysS cells and purified as described,[35] except that Hepes-based buffers without detergent were used.

Fluorescence labeling

Labeling of Ffh containing one or two cysteine residues with the maleimide derivatives of OG 488 or Bpy FL was carried out by reacting the protein with a fivefold excess of dye for five hours on ice. Unreacted dye was removed by gel-filtration through Sephadex G-25.

For 3′ end labeling, 4.5 S RNA or the 49mer/61mer fragments (100 A_{260} units/ml) was oxidized by incubation in 0.1 M sodium acetate (pH 5.3), 5 mM KIO_4 for 30 minutes at 0 °C in the dark. The reaction was stopped by adding ethylene glycol to a concentration of 10 mM and incubating further for five minutes at 0 °C. After precipitation in ethanol, RNA was dissolved in 0.1 M sodium acetate (pH 5.3) and reacted with a threefold excess of Alx555/647 hydrazide for five hours at 20 °C in the dark. To remove free dye, the RNA was extracted three times with phenol, precipitated three times with ethanol, and dissolved in 20 mM Hepes (pH 7.5), 7 mM magnesium acetate, 0.5 mM EDTA, 100 mM NH_4Cl. On the basis of absorbance measurements, the extent of labeling was about 90%. Labeled RNA was separated from unlabeled RNA by FPLC on MonoQ using a gradient from 0.5 M–0.8 M LiCl in 20 mM Hepes (pH 7.5), 7 mM magnesium acetate, 0.5 mM EDTA, 100 mM NH_4Cl. Fractions containing labeled RNA were pooled and RNA precipitated with ethanol. All labeled Ffh mutants and RNA constructs used in the present work were fully functional in forming the respective Ffh–RNA complexes, as assayed by gel mobility-shift electrophoresis (data not shown).[36]

Dibromobimane crosslinking

Double mutants Ffh(C231/377) and Ffh(C17/344) were reacted with a 1.1-fold molar excess of 4,6-bis(bromomethyl)-3,7-dimethyl-1,5-diazabicyclo [3.3.0]octa-3,6-diene-2,8-dione (dibromobimane, dBrB). Samples were withdrawn at different times, purified from unbound crosslinker by gel-filtration chromatography on Sephadex G-25, and fluorescence was measured (excitation 390 nm; emission 470 nm). Single cysteine mutants 231 or 377 were treated with a fivefold excess of mBrB and processed in the same way as the double mutant. For protease digestion analysis, bimane-labeled Ffh was purified by FPLC on MonoQ using a 0.25 M–0.30 M gradient of KCl in 20 mM Hepes (pH 7.5); fractions containing bimane-labeled proteins were identified by monitoring fluorescence.

Protease digestion assay

Digestions with V8 protease of purified bimane-reacted Ffh were carried out at room temperature in a final volume of 50–100 μl as described.[30] For SRP formation, equimolar amounts of 4.5 S RNA and Ffh were added. To monitor the time-course of digestion, 5 μl samples were withdrawn, mixed with loading buffer, boiled for five minutes, and stored on ice before analysis by SDS-PAGE.

FRET measurements

FRET efficiencies were determined from both steady-state fluorescence (intensity or anisotropy) and fluorescence lifetime measurements. Anisotropy was measured on a PTI QuantaMaster C-61/ 2000 T-Format scanning spectrofluorimeter with both excitation and emission light polarized with Glan-Thompson polarizers; measurements were carried out in buffer A in the presence of 60% or 90% (v/v) glycerol (20 °C) to eliminate the influence of protein rotation on the fluorescence

anisotropy (limiting anisotropy). Data were analyzed with FeliX TM software (PTI, Canada). Fluorescence decay experiments were carried out in buffer A containing 10% (v/v) glycerol at 20 °C. Time-domain lifetime measurements were carried out using a fluorescence lifetime spectrometer FluoTime 100 (PicoQuant GmbH, Germany). Excitation pulses (440 nm, 10 MHz, 60 ps width) were generated by a laser diode system (PTD 800B with LDH PC 440, PicoQuant GmbH, Germany). To avoid scattered light, a 500 nm liquid cut-off filter ($CrO_4^{2-}/Cr_2O_7^{2-}$, 0.3 M, basic pH) was used in the emission channel. Data analysis was performed using multi-exponential fluorescence decay fitting software FluoFit v. 3.2.0 (PicoQuant GmbH, Germany). For frequency-domain measurements, a 10 GHz instrument with picosecond time-resolution was used.[37,38] Briefly, the excitation was from a cavity-dumped DCM dye laser (frequency-doubled to 330 nm) pumped synchronously by a mode-locked argon ion laser. The detection system was a 6 μm microchannel plate (Hamamatsu). Frequency-domain data were evaluated in terms of one or two lifetimes.[37,38] Both methods, time-domain and frequency-domain, yielded the same lifetimes of unquenched donors. Lifetimes less than 1ns and complex decay curves were better resolved with the 10 GHz instrument. Fluorescence decay curves of samples with donor alone could be fully described by a single-exponential function. In the presence of donor and acceptor, two-exponential decay curves were observed in several cases; in these cases, average lifetimes, as summarized in the Tables, were used for the determination of FRET efficiencies.

The distances between fluorescent dyes, R, were estimated from FRET efficiencies, E, according to the following equations:[27]

$$E = R_0^6/(R_0^6 + R^6)$$

where R_0 is the distance at which 50% FRET efficiency is observed; FRET efficiencies were determined from the decrease of the fluorescence lifetime or intensity of the donor in the presence of acceptor, or from the anisotropy decrease observed in the presence of two identical fluorophores compared to one:

$$E = 1 - (\tau_{DA}/\tau_D)$$

$$E = 1 - (F_{DA}/F_D)$$

$$E = 2(r_{D0} - \langle r_{DD}\rangle)/r_{D0}$$

where τ_{DA}, F_{DA} and τ_D, F_D are the lifetimes and fluorescence intensities of the donor in the presence and in the absence of acceptor, respectively, and r_{D0} and r_{DD} are the limiting anisotropies of one fluorophore alone or two fluorophores, respectively. R_0 values for different donor–acceptor pairs were calculated using the equation:

$$R_0 = (8.79 \times 10^{-25})[n^{-4}Q\kappa^2 J(\lambda)]$$

where n is the refractive index ($n=1.4$ was used), Q is the quantum yield of the donor in the absence of acceptor, κ^2 is the orientation factor, and $J(\lambda)$ is the overlap integral between donor emission and acceptor absorption. $R_{0(2/3)}$ values (for $\kappa^2=2/3$) determined for the donor–acceptor pairs used in this work, in all cases determined for the fluorophores coupled to Ffh or RNA, are given in the text. Quantum yields were measured by comparison of the wavelength-integrated emission intensities of protein-bound fluorophores to that of a known standard as described;[27] the quantum yields of Bpy and OG attached to Ffh were 0.90 and 0.65, respectively.

Distance ranges due to the uncertainty about the orientation of the fluorophores were estimated from the ranges of κ^2 values, as determined from anisotropy measurements:[39]

$$R_{0min} = (3\kappa^2_{min}/2)^{1/6} \times R_{(2/3)}; \quad R_{0max} = (3\kappa^2_{max}/2)^{1/6} \times R_{(2/3)}$$

where $R_{(2/3)}$ is the distance calculated assuming $\kappa^2=2/3$:

$$\kappa^2_{min} = 2/3[1 - (d^x_D + d^x_A)/2]$$

$$\kappa^2_{max} = 2/3[1 + d^x_D + d^x_A + 3d^x_D d^x_A)/2]$$

where $d^x_i = (r_i/r_0)^{1/2}$ are depolarization factors, and r_i and r_0 the limiting and fundamental anisotropies, respectively, as determined from Perrin plots[27] for the fluorophores attached to Ffh or RNA, respectively (r_i/r_0): OG, 0.31/0.39; Bpy, 0.32/0.39; Alx555/647, 0.14/0.38 (49mer) or 0.10/0.38 (61mer, 4.5 S RNA).

Data analysis and modeling

To transform FRET distances into three-dimensional models of Ffh and SRP, we used a program, FRETsg,[40] that generates an ensemble of configurations of residues in space consistent with the experimentally determined distances between these positions. The program writes the models to a PDB-type file, which can be overlaid easily with other PDB structures. For each case, 2000 initial models were built, of which the best 50 were examined further. The uncertainty ranges of the FRET distances were included in the calculations as a "width" parameter attached to each distance value. The program yielded an ensemble of configurations represented as a file where the individual configurations were fit onto each other. This dataset was used to align models of 4.5 S RNA and crystal structures of the NG and M domains of Ffh as independent rigid bodies. An independent movement of the N domain was not required to fit the data.

Acknowledgements

We thank Carmen Schillings, Astrid Böhm, Simone Möbitz and Petra Striebeck for expert technical assistance. The work was supported by the Deutsche Forschungsgemeinschaft, the Alfried Krupp von Bohlen und Halbach-Stiftung, and the Fonds der Chemischen Industrie.

References

1. Keenan, R. J., Freymann, D. M., Stroud, R. M. & Walter, P. (2001). The signal recognition particle. *Annu. Rev. Biochem.* **70**, 755–775.
2. Nagai, K., Oubridge, C., Kuglstatter, A., Menichelli, E., Isel, C. & Jovine, L. (2003). Structure, function and evolution of the signal recognition particle. *EMBO J.* **22**, 3479–3485.
3. Doudna, J. A. & Batey, R. T. (2004). Structural insights into the signal recognition particle. *Annu. Rev. Biochem.* **73**, 539–557.
4. Rosenblad, M. A., Gorodkin, J., Knudsen, B., Zwieb, C. & Samuelsson, T. (2003). SRPDB: signal recognition particle database. *Nucl. Acids Res.* **31**, 363–364.

5. Krieg, U. C., Walter, P. & Johnson, A. E. (1986). Photocrosslinking of the signal sequence of nascent preprolactin to the 54-kilodalton polypeptide of the signal recognition particle. *Proc. Natl Acad. Sci. USA*, **83**, 8604–8608.
6. Kurzchalia, T. V., Wiedmann, M., Girshovich, A. S., Bochkareva, E. S., Bielka, H. & Rapoport, T. A. (1986). The signal sequence of nascent preprolactin interacts with the 54K polypeptide of the signal recognition particle. *Nature*, **320**, 634–636.
7. Connolly, T., Rapiejko, P. J. & Gilmore, R. (1991). Requirement of GTP hydrolysis for dissociation of the signal recognition particle from its receptor. *Science*, **252**, 1171–1173.
8. Gu, S. Q., Peske, F., Wieden, H. J., Rodnina, M. V. & Wintermeyer, W. (2003). The signal recognition particle binds to protein L23 at the peptide exit of the *Escherichia coli* ribosome. *RNA*, **9**, 566–573.
9. Keenan, R. J., Freymann, D. M., Walter, P. & Stroud, R. M. (1998). Crystal structure of the signal sequence binding subunit of the signal recognition particle. *Cell*, **94**, 181–191.
10. Ramirez, U. D., Minasov, G., Focia, P. J., Stroud, R. M., Walter, P., Kuhn, P. & Freymann, D. M. (2002). Structural basis for mobility in the 1.1 Å crystal structure of the NG domain of *Thermus aquaticus* Ffh. *J. Mol. Biol.* **320**, 783–799.
11. Freymann, D. M., Keenan, R. J., Stroud, R. M. & Walter, P. (1997). Structure of the conserved GTPase domain of the signal recognition particle. *Nature*, **385**, 361–364.
12. Montoya, G., Kaat, K., Moll, R., Schafer, G. & Sinning, I. (2000). The crystal structure of the conserved GTPase of SRP54 from the archaeon *Acidianus ambivalens* and its comparison with related structures suggests a model for the SRP–SRP receptor complex. *Struct. Fold. Des.* **8**, 515–525.
13. Padmanabhan, S. & Freymann, D. M. (2001). The conformation of bound GMPPNP suggests a mechanism for gating the active site of the SRP GTPase. *Structure (Camb)*, **9**, 859–867.
14. Clemons, W. M., Jr, Gowda, K., Black, S. D., Zwieb, C. & Ramakrishnan, V. (1999). Crystal structure of the conserved subdomain of human protein SRP54M at 2.1 Å resolution: evidence for the mechanism of signal peptide binding. *J. Mol. Biol.* **292**, 697–705.
15. Batey, R. T., Rambo, R. P., Lucast, L., Rha, B. & Doudna, J. A. (2000). Crystal structure of the ribonucleoprotein core of the signal recognition particle. *Science*, **287**, 1232–1239.
16. Kuglstatter, A., Oubridge, C. & Nagai, K. (2002). Induced structural changes of 7SL RNA during the assembly of human signal recognition particle. *Nature Struct. Biol.* **9**, 740–744.
17. Batey, R. T., Sagar, M. B. & Doudna, J. A. (2001). Structural and energetic analysis of RNA recognition by a universally conserved protein from the signal recognition particle. *J. Mol. Biol.* **307**, 229–246.
18. Rosendal, K. R., Wild, K., Montoya, G. & Sinning, I. (2003). Crystal structure of the complete core of archaeal signal recognition particle and implications for interdomain communication. *Proc. Natl Acad. Sci. USA*, **100**, 14701–14706.
19. Larsen, N. & Zwieb, C. (1991). SRP-RNA sequence alignment and secondary structure. *Nucl. Acids Res.* **19**, 209–215.
20. Gorodkin, J., Knudsen, B., Zwieb, C. & Samuelsson, T. (2001). SRPDB (Signal Recognition Particle Database). *Nucl. Acids Res.* **29**, 169–170.
21. Poritz, M. A., Strub, K. & Walter, P. (1988). Human SRP RNA and *E. coli* 4.5 S RNA contain a highly homologous structural domain. *Cell*, **55**, 4–6.
22. Bourgaize, D. B., Farrell, C., Langley, K. H. & Fournier, M. J. (1984). Physical properties of the *E. coli* 4.5 S RNA: first results suggest a hairpin helix of unusual thermal stability. *Nucl. Acids Res.* **12**, 2019–2034.
23. Lentzen, G., Dobberstein, B. & Wintermeyer, W. (1994). Formation of SRP-like particle induces a conformational change in *E. coli* 4.5 S RNA. *FEBS Letters*, **348**, 233–238.
24. Lentzen, G., Moine, H., Ehresmann, C., Ehresmann, B. & Wintermeyer, W. (1996). Structure of 4.5 S RNA in the signal recognition particle of *Escherichia coli* as studied by enzymatic and chemical probing. *RNA*, **2**, 244–253.
25. Buskiewicz, I., Kubarenko, A., Peske, F., Rodnina, M. V. & Wintermeyer, W. (2005). Domain rearrangement of SRP protein Ffh upon binding 4.5 S RNA and the SRP receptor FtsY. *RNA*, **11**, 947–957.
26. Gu, S. Q., Jöckel, J., Beinker, P., Warnecke, J., Semenkov, Y. P., Rodnina, M. V. & Wintermeyer, W. (2005). Conformation of 4.5 S RNA in the signal recognition particle and on the 30 S ribosomal subunit. *RNA*, **11**, in the press.
27. Lakowicz, J. R. (1999). *Principles of Fluorescence Spectroscopy* (3rd edit.), Kluwer Academic/Plenum Publishers, New York pp. 305–309.
28. Weber, G. & Shinitzky, M. (1970). Failure of energy transfer between identical aromatic molecules on excitation at the long wave edge of the absorption spectrum. *Proc. Natl Acad. Sci. USA*, **65**, 823–830.
29. Mornet, D., Ue, K. & Morales, M. F. (1985). Stabilization of a primary loop in myosin subfragment 1 with a fluorescent crosslinker. *Proc. Natl Acad. Sci. USA*, **82**, 1658–1662.
30. Zheng, N. & Gierasch, L. M. (1997). Domain interactions in *E. coli* SRP: stabilization of M domain by RNA is required for effective signal sequence modulation of NG domain. *Mol. Cell*, **1**, 79–87.
31. Egea, P. F., Shan, S. O., Napetschnig, J., Savage, D. F., Walter, P. & Stroud, R. M. (2004). Substrate twinning activates the signal recognition particle and its receptor. *Nature*, **427**, 215–221.
32. Focia, P. J., Shepotinovskaya, I. V., Seidler, J. A. & Freymann, D. M. (2004). Heterodimeric GTPase core of the SRP targeting complex. *Science*, **303**, 373–377.
33. Halic, M., Becker, T., Pool, M. R., Spahn, C. M., Grassucci, R. A., Frank, J. & Beckmann, R. (2004). Structure of the signal recognition particle interacting with the elongation-arrested ribosome. *Nature*, **427**, 808–814.
34. Rinke-Appel, J., Osswald, M., von Knoblauch, K., Mueller, F., Brimacombe, R., Sergiev, P. *et al*. (2002). Crosslinking of 4.5 S RNA to the *Escherichia coli* ribosome in the presence or absence of the protein Ffh. *RNA*, **8**, 612–625.
35. Jagath, J. R., Rodnina, M. V. & Wintermeyer, W. (2000). Conformational changes in the bacterial SRP receptor FtsY upon binding of guanine nucleotides and SRP. *J. Mol. Biol.* **295**, 745–753.
36. Jagath, J. R., Matassova, N. B., de Leeuw, E., Warnecke, J. M., Lentzen, G., Rodnina, M. V. *et al*. (2001). Important role of the tetraloop region of 4.5 S RNA in SRP binding to its receptor FtsY. *RNA*, **7**, 293–301.
37. Laczko, G., Gryczynski, I., Gryczynski, Z., Wiczk, W.,

Malak, H. & Lakowicz, J. R. (1990). A 10 GHz frequency-domain instrument. *Rev. Sci. Instrum.* **61**, 2331–2337.
38. Lakowicz, J. R. & Gryczynski, I. (1991). Frequency-domain fluorescence spectroscopy. In *Topics in Fluorescence Spectroscopy* (Lakowicz, J. R., ed.), vol. 1, pp. 293–335, Plenum Press, New York.
39. Lakowicz, J. R., Gryczynski, I., Cheung, H. C., Wang, C. K., Johnson, M. L. & Joshi, N. (1988). Distance distributions in proteins recovered by using frequency-domain fluorometry. Applications to troponin I and its complex with troponin C. *Biochemistry*, **27**, 9149–9160.
40. Schröder, G. F. & Grubmüller, H. (2004). FRETsg: biomolecular structure model building from multiple FRET experiments. *Comput. Phys. Com.* **158**, 150–157.

Edited by D. E. Draper

(Received 19 April 2005; received in revised form 6 June 2005; accepted 7 June 2005)

Available online 24 June 2005